Nuclear Mathematical and Computational Sciences: A Century in Review, A Century Anew
Gatlinburg, Tennessee, April 6-11, 2003, on CD-ROM, American Nuclear Society, LaGrange Park, IL (2003)

MONTE CARLO ELECTRON DOSE CALCULATIONS USING DISCRETE SCATTERING ANGLES AND DISCRETE ENERGY LOSSES

Brian C. Franke
Sandia National Laboratories
P.O. Box 5800, Albuquerque, NM 87185-1179
bcfrank@sandia.gov

Anil K. Prinja
University of New Mexico
Chemical and Nuclear Engineering Department
209 Farris Engineering Center, Albuquerque, NM 87131
prinja@unm.edu

ABSTRACT

We present a computationally efficient transport-based method for calculating dose from electrons. The exact elastic scattering and inelastic energy-loss cross sections for electrons are converted into discrete angular-deflections and discrete energy-losses, which are constrained to exactly preserve the low-order moments of the analog cross sections. This method is implemented using realistic electron cross sections based on the screened Rutherford angular scattering cross section and the Rutherford energy-loss cross section. However, the method is based on only the cross section moments and may be extended to any angular and energy scattering models for which the moments are known.

By comparison with analog Monte Carlo calculations, we demonstrate that few discrete angles and energies are required to achieve accurate dose distributions, and the calculations are fast. The method can yield accurate results across the entire spatial extent of the transport problem for a wide range of problems, from relatively isotropic scattering (keV electrons in high-Z material) to highly forward-peaked scattering (MeV electrons in low-Z material). We also illustrate that this method incurs no inaccuracies from the presence of a material interface. The computational efficiency of the method is compared with analog calculations.

Key Words: Monte Carlo, Electron Transport, Dose

1. INTRODUCTION

Simulation of energetic electron transport in amorphous media by analog Monte Carlo methods is computationally very demanding and inefficient because of the long range Coulomb forces which mediate charged particle interactions. The associated large elastic and inelastic scattering cross sections lead to thousands of collisions per electron history, while angular deflections and energy losses are highly peaked about forward directions and vanishing small energy transfers. The condensed history Monte Carlo method [1] provides a practical alternative for simulating electron transport on complex geometries with realistic physics and forms the basis of most of the charged particle production codes currently in use [2–5]. In this method, the electron is moved in fixed, predetermined steps and angular deflections and energy losses are sampled from precomputed step-size dependent distributions obtained from multiple scattering theories. These theories assume that scattering is sufficiently forward peaked and the step size sufficiently small that the particle path length is indistinguishable from its actual displacement. While the

method has been extensively analyzed [6] and elaborate schemes proposed to relax the step size restriction [7], fundamental deficiencies remain. In particular, stepping across material interfaces requires special care with this method, since the multiple scattering theories are valid for infinite media only. Furthermore, the approach becomes less efficient with decreasing scattering anisotropy, when the distinction between path length and actual displacement becomes increasingly important.

The complexity of the condensed history algorithm stands in contrast to the simplicity of analog Monte Carlo simulation, and recently there has been much interest in constructing effective transport formulations [8–11] which correctly describe the underlying tranport mechanics (in particular, the Markovian feature of exponentially distributed collision sites is restored). A common feature in these new approaches is that the underlying interaction physics is approximated in a systematic manner to yield longer mean free paths and smoother deflection and energy loss distributions, which makes it practical to simulate transport by single event Monte Carlo. Accuracy is controlled by enforcing the preservation of important physical information, such as a sufficient number of Lewis moments [12]. For elastic scattering, this approach has been implemented in a particularly efficient manner in [11, 13] where a discrete scattering-angle formulation was developed and demonstrated to yield accurate results for the angular distribution and radial spread of an electron pencil beam.

With the exception of [10], effective or renormalized transport models that incorporate energy-loss straggling have not been developed. In this article we generalize the approach of [11] by constructing a discrete energy-loss formulation which preserves important energy-loss moments of the analog inelastic cross section. This approach successively yields the correct mean energy-loss (the stopping power), the mean-square energy-loss (the straggling coefficient) and higher order moments to any desired order. We demonstrate that this representation of inelastic interactions, in conjunction with the discrete scattering-angle representation of elastic scattering, yields a fast and accurate method for computing electron dose distributions using single event Monte Carlo.

The scope of the article is as follows. In Section 2, we introduce the analog problem for transport of electron pencil beams in amorphous media and present the reduced descriptions obtained using discrete scattering-angle and energy-loss formulations. In Section 3, Monte Carlo numerical results for dose-depth distributions (i.e. one-dimensional energy deposition profiles) for various orders of the discrete representation are presented and compared with results obtained for the analog problem. Differences in runtimes are also discussed. In Section 4, we demonstrate the accuracy of our approach in another dimension by comparing calculated doses as a function of radius. The article concludes with some final remarks in Section 5.

2. DISCRETE SCATTERING MODELS

We consider a monoenergetic electron beam incident on a slab of material. The angular flux $\psi(\vec{r},\vec{\Omega},E)$ of electrons at spatial location $\vec{r}(x,y,z)$ traveling along direction $\vec{\Omega}(\mu,\phi)$ with energy E satisfies the linear transport equation given in standard notation by,

$$\vec{\Omega}\cdot\nabla\psi(\vec{r},\vec{\Omega},E)=\int_0^\infty\int_{4\pi}\sigma_s(\vec{r},\vec{\Omega}\cdot\vec{\Omega}',E'\rightarrow E)\,\psi(\vec{r},\vec{\Omega}',E')d\vec{\Omega}'dE'-\sigma_s(\vec{r},E)\,\psi(\vec{r},\vec{\Omega},E), \qquad (1)$$

with a pencil beam incident on the left face along the z-axis,

$$\psi(x,y,0,\mu,\phi,E)=\frac{1}{2\pi}\delta(\mu-1)\,\delta(E-E_0)\,\delta(x)\,\delta(y),\quad \mu>0, \qquad (2)$$

and vacuum boundary condition on the right face,

$$\psi(x, y, Z, \mu, \phi, E) = 0, \quad \mu < 0. \tag{3}$$

In electron-target atom interactions, elastic and inelastic interactions are handled independently. Furthermore, elastic collisions are assumed to occur without energy loss and inelastic collisions without angular deflection. Under these conditions, the transport equation becomes,

$$\begin{aligned} \vec{\Omega} \cdot \nabla \psi(\vec{r}, \vec{\Omega}, E) &= \int_{4\pi} \sigma_{s,el}(\vec{r}, \vec{\Omega} \cdot \vec{\Omega}', E)\, \psi(\vec{r}, \vec{\Omega}', E) d\vec{\Omega}' \\ &+ \int_0^\infty \sigma_{s,in}(\vec{r}, E' \to E)\, \psi(\vec{r}, \vec{\Omega}, E') dE' \\ &- [\sigma_{s,el}(\vec{r}, E) + \sigma_{s,in}(\vec{r}, E)]\, \psi(\vec{r}, \vec{\Omega}, E). \end{aligned} \tag{4}$$

The elastic scattering differential cross section (DCS) is accurately described by the Mott cross section at high energies and correspondingly by the Möller cross section for inelastic interactions [14]. As mentioned previously, these differential cross sections are highly peaked about $\vec{\Omega} \cdot \vec{\Omega}' \equiv \mu_0 = 1$ and $E' - E = 0$ while the total scattering cross section $\sigma_s(\vec{r}, E) \gg 1$. The high frequency of electron-target atom collisions, coupled with miniscule changes in the electron state per collision, is the underlying cause of the inefficiency of analog electron Monte Carlo simulations. In the next section we describe our reduced transport model based on moment-preserving discrete scattering representations, which, in subsequent sections, is demonstrated to be a viable and practical alternative to analog Monte Carlo calculations of electron dose.

2.1. Angular Scattering

To introduce our approach to angular scattering, we define *momentum transfer* moments of the elastic DCS according to

$$\sigma_{n,el}(\vec{r}, E) = 2\pi \int_{-1}^{1} d\mu_0\, (1 - \mu_0)^n \sigma_{s,el}(\vec{r}, \mu_0, E), \quad n = 1, 2, \ldots \tag{5}$$

Note that unlike the traditional Legendre moments, the momentum transfer moments $\sigma_{n,el}$ are all positive for a positive DCS and, moreover, for a sufficiently peaked DCS, they form a rapidly decreasing sequence. Thus, in a sense (made more precise below) the $\sigma_{n,el}$ provide a natural characterization of forward peaked scattering, as the Legendre moments do for nearly isotropic scattering. We also note that $\sigma_{1,el}$ is just the familiar transport cross section.

The essence of our method is to replace $\sigma_{s,el}(\vec{r}, \mu_0, E)$ by an approximate DCS, $\tilde{\sigma}_{s,el}(\vec{r}, \mu_0, E)$, defined such that the associated momentum transfer moments $\tilde{\sigma}_{n,el}$ are identical to the exact moments $\sigma_{n,el}$ for $n = 1, 2 \ldots N$, where N is arbitrary but finite. All higher moments $\{\tilde{\sigma}_{n,el},\ n = N+1, N+2 \ldots\}$ are approximated in terms of these lower moments. The motivation and expectation is that by not rigorously preserving all momentum transfer moments we are modeling an effectively less singular scattering process. The consequence is that the reduced physics should yield a longer mfp than the actual mfp as well as a less peaked post-collision angular distribution. On the other hand, strictly preserving a number of lower order moments should provide accuracy. This approach was motivated by the observation that the Fokker-Planck approximation to the elastic scattering operator (i) only preserves the first moment $\sigma_{1,el}$ yet is extensively used for pencil beams, forming the basis of the well known Fermi and Fermi-Eyges solutions, and (ii) constitutes the lowest order in a Generalized Fokker-Planck (GFP) expansion whose coefficients depend on

the $\sigma_{n,el},\ n \geq 1$ [9, 15, 16]. Moreover, Lewis theory [12] clearly demonstrates a direct correlation between preserving moments of the DCS and model accuracy as measured by space-angle moments of the infinite medium solution. This suggests that increasingly more accurate physics can be captured by preserving increasingly higher-order moments. However, it was shown in [16] that the GFP expansion is asymptotic, being unstable to truncation orders beyond Fokker-Planck. Higher order moments cannot, therefore, be preserved by retaining only a finite number of terms in this expansion. An alternative approach was presented in [9] where the GFP expansion was first renormalized to yield a convergent series and then converted by resummation to an integral scattering operator possessing a smoother scattering kernel. However, this approach [9] does not yield an explicit, effective differential cross section, rather it gives the coefficients of a spherical harmonics expansion of the cross section, which is not convenient for sampling deflection angles in a Monte Carlo simulation.

We adopt a conceptually simpler approach in which $\tilde{\sigma}_{s,el}$ is represented as a superposition of discrete scattering angles, that is,

$$\tilde{\sigma}_{s,el}(\vec{r}, \mu_0, E) = \sum_{l=1}^{L} \frac{\alpha_l(\vec{r}, E)}{2\pi} \delta\left[\mu_0 - \xi_l(\vec{r}, E)\right]. \tag{6}$$

The scattering amplitudes $\{\alpha_l,\ l = 1, 2 \ldots\ L\}$ and scattering cosines $\{\xi_l,\ l = 1, 2 \ldots\ L\}$ are constrained to yield the exact first $2L$ momentum transfer moments $\{\sigma_{l,el},\ l = 1, 2 \ldots 2L\}$ as given by Eq.(5). This condition yields a nonlinear algebraic system for the α_l and ξ_l that can be solved by an existing method using Radau quadrature developed by Sloan [17]. It has been observed to be robust for a wide range of physics and $L \leq 8$. Sampling precalculated scattering angles using Eq.(6) is almost trivial, which is an important consideration in the overall efficiency of Monte Carlo simulations.

For $L = 1$, only the transport cross section $\sigma_{1,el}$ and the mean square momentum transfer $\sigma_{2,el}$ are rigorously preserved, but for extremely forward peaked scattering this may prove sufficient. Notice, in this case, that if the limit $\xi_1 \to 1$ is taken while simultaneously enforcing the requirement that the correct transport cross section be obtained, the Fokker-Planck approximation is realized. Setting ξ_1 close to unity then gives Morel's discrete representation of the Fokker-Planck approximation [18], which provides a practical method for simulating Fokker-Planck scattering by Monte Carlo.

The mfp corresponding to L discrete directions is given by $\tilde{\lambda}_L = \left(\sum_{l=1}^{L} \alpha_l\right)^{-1}$ and can be used as a measure of the potential speed-up over the analog case. For illustration, we consider 1 MeV electrons incident on a gold target with elastic scattering described by the screened Rutherford DCS [19]. The screening parameter at this energy is $\eta = 8.884 \times 10^{-5}$ which corresponds to a mean cosine of scattering $\bar{\mu}_0 = 0.99852$ and a mfp $\lambda = 6.82 \times 10^{-6}$ cm. This yields $\tilde{\lambda}_1/\lambda = 162$, $\tilde{\lambda}_2/\lambda = 59$, and $\tilde{\lambda}_4/\lambda = 23$, and indicates that considerable reduction in the average number of collisions per history is realizable with the moment preserving method.

2.2. Energy Scattering

It was shown in [10] that the inelastic energy loss process and the elastic angular scattering process shared important characteristics. In particular, the large total inelastic cross section and the high probability of very small energy transfers gives a GFP expansion in energy that is analogous to the angular expansion in [9] and is unstable or divergent when truncated beyond strictly Fokker-Planck. However, in the Fokker-Planck approximation, only the mean and mean square energy loss per unit path length travelled

can be preserved. It was further demonstrated that just as in [9], the GFP expansion could be renormalized to yield a stable expansion to all orders such that energy-loss moments up to a desired order were identical to the analog or exact values. This expansion was then reduced to an effective integral inelastic scattering operator with an explicit energy loss kernel that was easy to sample from [10]. Numerical results showed that preserving four energy-loss moments were sufficient to yield extremely accurate energy spectra for even very thin targets.

Here we further extend the analogy to elastic scattering and develop a discrete energy loss model for inelastic interactions also. The energy-loss moments of the inelastic DCS are defined by,

$$\sigma_{n,in}(\vec{r},E) = \int_0^E dE' \, (E-E')^n \sigma_{s,in}(\vec{r},E \to E'), \quad n = 1,2,\ldots \tag{7}$$

We then approximate the inelastic DCS by a discrete energy-loss model,

$$\tilde{\sigma}_{s,in}(\vec{r},E') = \sum_{l=1}^{L} \frac{\beta_l(\vec{r},E)}{2\pi} \, \delta\left[E' - \zeta_l(\vec{r},E)\right], \tag{8}$$

where the amplitudes $\{\beta_l,\, l = 1,2\ldots\ L\}$ and energy-losses $\{\zeta_l,\, l = 1,2\ldots\ L\}$ are constrained to yield the exact first $2L$ energy-loss moments $\{\sigma_{l,in},\, l = 1,2\ldots 2L\}$. All higher moments $\{\tilde{\sigma}_{n,in},\, n = N+1, N+2\ldots\}$ are then expressed in terms of these lower moments. Thus, for $L = 1$ (i.e. a single discrete term) the correct stopping power and straggling coefficient are obtained. It is important to note that unlike the Fokker-Planck approximation for straggling, all higher energy-loss moments are accounted for in the discrete representation, albeit approximately. Moreover, the discrete model yields a strictly downscatter representation of energy loss, faithful to the analog process, while the FP model, which approximates straggling as a diffusion in energy, yields upscatter as well. We conclude that the discrete energy-loss model for $L = 1$ has potential accuracy exceeding that of the Fokker-Planck approximation with the same stopping power and straggling coefficient.

The parameters $\{\beta_l,\, \zeta_l\}$ in Eq.(8) are obtained by constructing an invertible linear mapping of the discrete energy-loss representation to a pseudo-elastic scattering representation similar to Eq.(6). The procedure outlined in [17] is then used to compute the parameters of the pseudo-process and the inverse mapping finally gives $\{\beta_l,\, \zeta_l\}$.

2.3. Calculation Methods

The calculations presented are conducted with simplified physics both for simplicity of implementation and to isolate the effects of the algorithms being tested. No secondary photons or electrons are simulated. Angular scattering is modeled using the screened Rutherford scattering model [19]. The discrete approximation requires only cross section moments, so the more accurate Mott [14] cross sections can be simulated also, but the analog benchmark is easier to obtain for the screened Rutherford case. The angular deflection of the primary electron due to inelastic scattering is not simulated, although a common approximation is to include it in the angular scattering cross section moments without correlation to energy loss [19]. The energy scattering is modeled as Rutherford scattering [19]. The moments of the more accurate Möller [14] cross section can easily be used in the discrete model, but the analog benchmark is easier to obtain for the Rutherford scattering model.

The energy dependence of the simulation is accomplished via physics parameters on an energy grid. These parameters are generated by the XGEN cross section generating code [2]. The grid is logarithmically

distributed with 8 values for every halving of energy. The physical parameters used by the code are the screening parameter, total elastic scattering cross section, and energy-loss moments (calculated from the mean excitation energy, density, atomic weight, and atomic number of the material). The discrete angle and discrete energy scattering parameters (α_l, ξ_l, β_l, and ζ_l) are precalculated on the energy grid. The electron transport code uses these parameters based on the nearest grid point to the energy of the particle. (A more sophisticated interpolation method could be employed.) In the calculations discussed here, the cutoff energy is set at one percent of the source energy or at two times the mean excitation energy, whichever is greater.

3. DEPTH DOSE PROFILES

In this section we present one-dimensional results from three different sets of calculations. The results are based on calculating the transversely-integrated dose in layers within the slabs of materials. In the following discussion of computational results, ”analog” refers to the transport simulation of angular scattering using the total elastic scattering cross sections with sampling from the screened Rutherford distribution and the simulation of energy scattering with sampling from the Rutherford distribution. ”Analog CSD” refers to the simulation of analog angular scattering, but with energy loss applied continuously based on the stopping power. ”N angles, M energies” means that N discrete scattering angles and M discrete energy-loss cross sections were calculated at each energy grid point.

3.1. Low-Energy, High-Z Calculation

First, we illustrate that this method can generate accurate results in a regime of relatively isotropic scattering. This is a regime in which traditional condensed history transport methods have some difficulty [8]. We simulated 250 keV electrons incident on a 0.008 cm thick slab of gold. In Fig. 1, the dose is shown as a function of depth for analog and approximate simulations. Some discrepencies can be seen between the analog result and the ”1 angle, 1 energy” model, but no significant discrepancies can be seen between the analog result and the ”2 angle, 2 energies” model.

In Fig. 2, the relative error in the approximate simulation as compared to the analog simulation is shown for several levels of approximation. The ”analog CSD” results are inaccurate at large depths due to the lack of energy straggling. The ”1 angle, 1 energy” model lacks energy straggling at large depths and is inaccurate at shallow depths due to the single scattering angle. The ”2 angles, 2 energies” model gives very good results even at large depths where the small doses recorded cause large statistical fluctuations in the comparison.

3.2. High-Energy, Low-Z Calculation

Next, we illustrate that this method can generate accurate results in a regime of highly forward-peaked scattering. This is a regime in which traditional condensed history transport methods perform quite well. Energy-loss straggling is more pronounced in such problems. We simulated 20 MeV electrons incident on a 30 cm thick slab of water. In Fig. 3, the dose is shown as a function of depth for an analog simulation. The inaccuracy of the analog CSD results shows the significance of energy straggling. Some discrepencies can be seen between the analog result and the ”1 angle, 1 energy” model, but no significant discrepancies can be seen between the analog result and the ”2 angles, 2 energies” model. Fig. 4 (the same results as

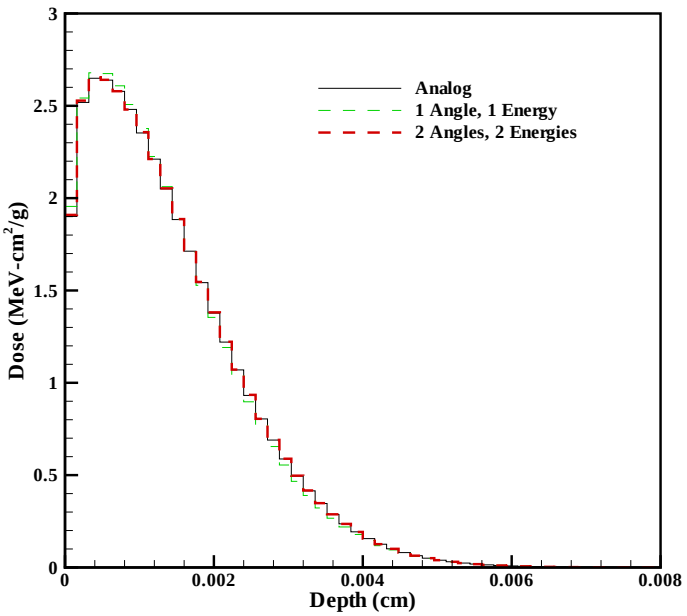

Figure 1. Dose from 250 keV electrons on gold.

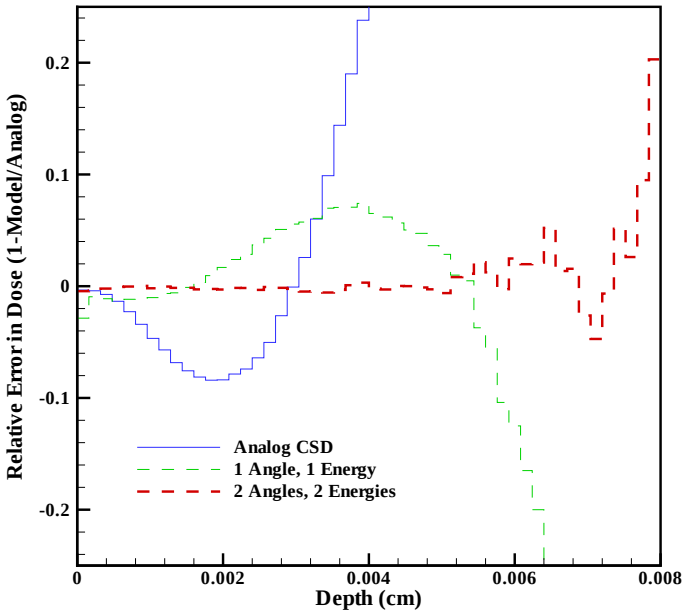

Figure 2. The relative error (in dose from 250 keV electrons on gold) of approximate models compared with analog Monte Carlo results.

Fig. 3 but on a logarithmic scale) shows that the ”2 angles, 2 energies” model is accurate even at depths where the dose is several orders of magnitude lower than the peak dose.

In Fig. 5, the relative error of the simulations is shown for several levels of approximation. All of the

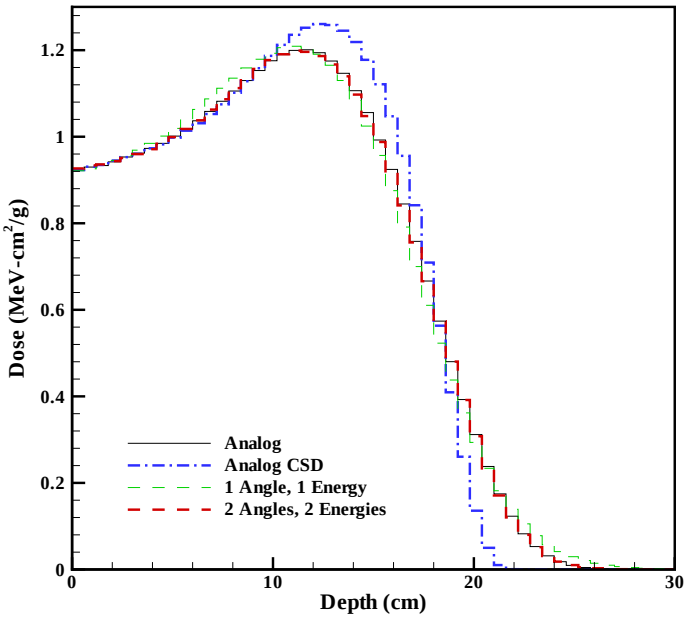

Figure 3. Dose from 20 MeV electrons on water.

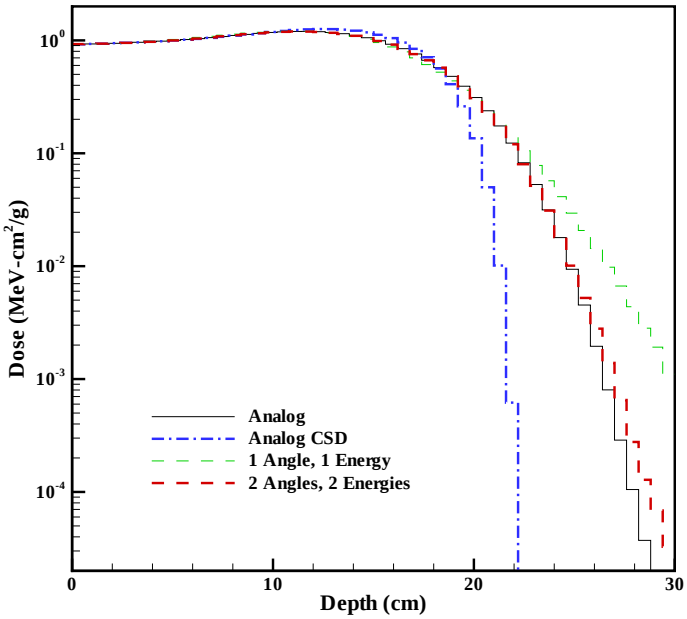

Figure 4. Dose from 20 MeV electrons on water.

simulations perform well at shallow depths, with some minor oscillations in the case of low-order angular approximations. At large depths the accuracy appears to be dominated by high-order energy-loss moments. The ”2 angles, 2 energies” model shows some oscillations at large depths. The ”4 angles, 4 energies” model is accurate across the slab, with the divergence at large depths being attributable to poor statistics in both the model simulation and the analog benchmark simulation.

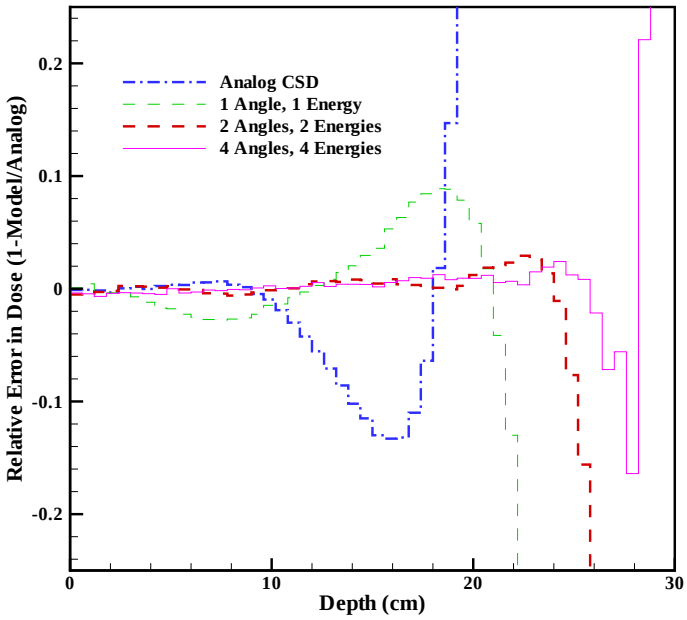

Figure 5. The relative error (in dose from 20 MeV electrons on water) of approximate models compared with analog Monte Carlo results.

Highly forward-peaked scattering is where this method has the largest speed-up factors relative to analog Monte Carlo calculations. The runtimes of the calculations were recorded. Table I shows the speed-up factors (i.e. the ratio of the runtimes) of this method for various degrees of approximation for both this high-energy case, the more isotropic low-energy case in the previous section, and two other intermediate cases. Even the accurate calculations yielded by the ”4 angles, 4 energies” approximation show a tremendous speed-up over analog calculations in the high-energy case. In the low-energy case, the speed-up is not as significant, but as was shown in Fig. 2, the ”2 angles, 2 energies” approximation may yield sufficient accuracy in that regime.

Table I. Speed-up of Discrete Method Over Analog Monte Carlo.

Order of Approximations	Speed-up Factor			
	20 MeV on Water	1 MeV on Water	1 MeV on Gold	250 keV on Gold
1 angle, 1 energy	1185.0	97.1	59.8	20.0
2 angles, 2 energies	450.4	41.6	26.7	9.4
4 angles, 4 energies	170.1	18.1	12.5	5.0

3.3. Material Interface Calculation

In this section, we illustrate that because the discrete approximation preserves the transport mechanics of the physical process, there are no observable effects due to material interfaces. This requires no special boundary crossing mechanics unique to material interfaces. The problem examined is 150 keV electrons

incident on a high-Z/low-Z interface (a 0.0004 cm layer of gold followed by a 0.0096 cm layer of aluminum). A similar problem was analyzed in [8] and compared with condensed history results. The dose as a function of depth is shown in Fig. 6. The relative errors of the approximate methods compared to the analog results are shown in Fig. 7. In the plot of the relative error, some inaccuracies are observable in the gold due to low-order angular approximations, but the ”4 angles, 4 energies” approximation is accurate throughout the problem.

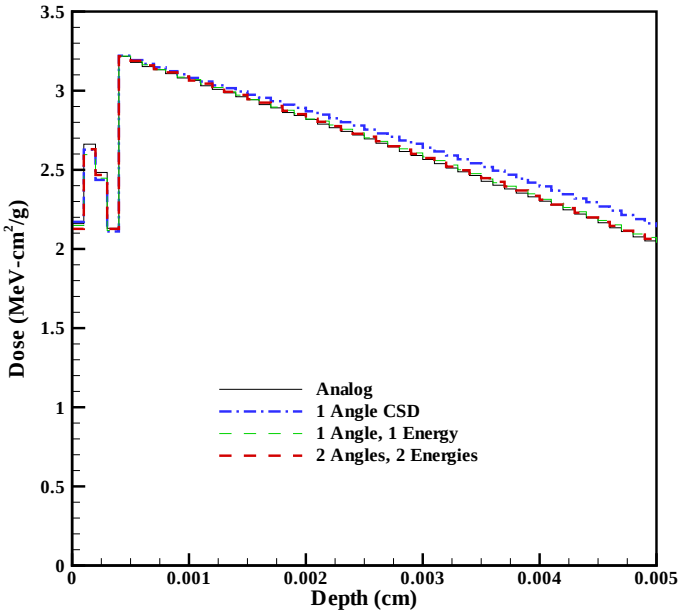

Figure 6. Dose from 150 keV electrons on gold/aluminum interface.

4. RADIAL DOSE PROFILES

In this section, we examine dose as a function of radius, both to illustrate the accuracy of the method in another dimension and to give further evidence of the lack of interface effects. For the gold-aluminum interface problem with a pencil beam source of normal incidence at zero radius, Fig. 8 shows the dose as a function of radius in aluminum. The results are for a depth between 0.0006 and 0.0008 cm. The relative errors of the approximate methods compared to the analog results are shown in Fig. 9. The speed-up produced by this method is due to a decrease in the total interaction cross section. As expected, this leads to an over-estimation of the uncollided flux. For low-order approximations, this effect is apparent in an over-estimation of dose at small radii. For high-order approximations, the total interaction cross section is still quite large, and the uncollided flux is only significant at very shallow depths. The over-estimation of other (once-collided, twice-collided, etc.) components of the flux is not apparent in a dose calculation. Even the over-estimation of the uncollided flux is not likely to be significant in calculations with a source of electrons distributed in angle, space, and energy, such as secondary electrons generated by photon interactions. For photon source calculations, even the ”1 angle, 1 energy” approximation may often produce acceptable results.

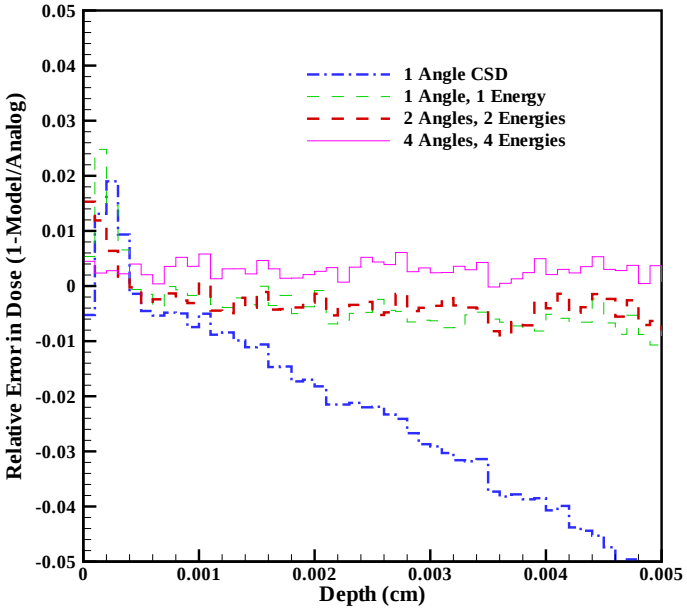

Figure 7. Relative error (in dose from 150 keV electrons on gold/aluminum interface) of approximate models compared with analog Monte Carlo results.

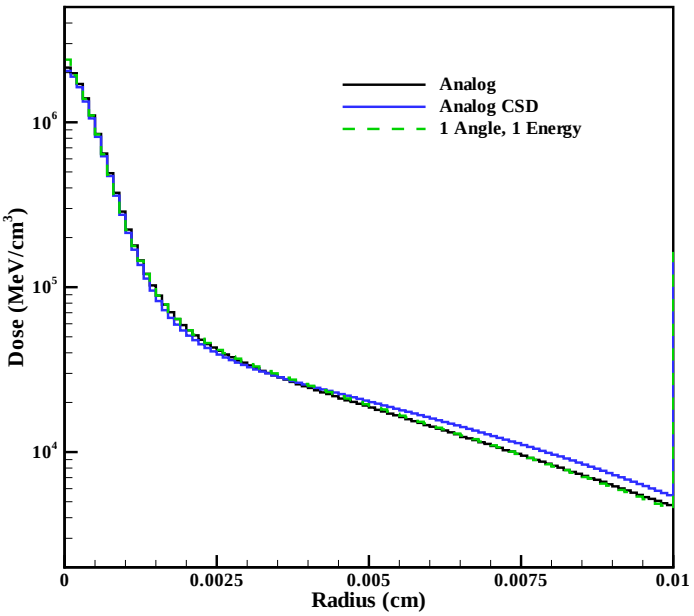

Figure 8. Radial distribution of dose from 150 keV electrons behind a gold/aluminum interface.

5. CONCLUSIONS

We have presented an approximate transport model for rapid and accurate electron dose calculations. Longer electron mean free paths than the corresponding analog values and the use of discrete scattering

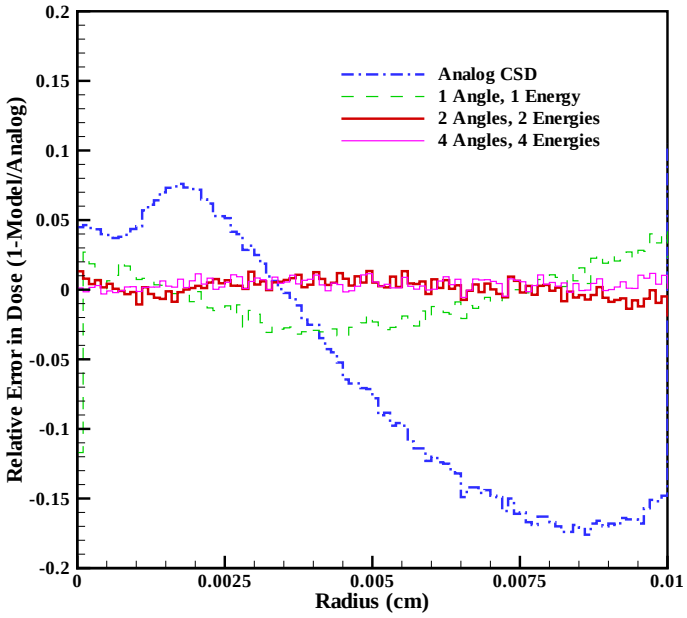

Figure 9. Relative error (in radial distribution of dose from 150 keV electrons behind a gold/aluminum interface) of approximate models compared with analog Monte Carlo results.

angle and energy-loss formulations for the elastic and inelastic collision integrals lead to efficient numerical implementation using single event Monte Carlo. It has been shown that this method is much faster than analog Monte Carlo for highly forward-peaked scattering. While the speed-up is not as significant for relatively isotropic scattering at low energies, it remains accurate in both regimes. Furthermore, no observable inaccuracies are introduced due to material interfaces.

No observable artifacts, such as ray effects, from the discrete energy-angle representation were apparent in the dose distribution for the cases considered. However, ray effects have previously been noted to occur in the angular distribution for very thin slabs [11] but a successful mitigation scheme was demonstrated [13] and others are known [20, 21]. Although we have not investigated this to date, “ray effects” resulting from discrete energy losses conceivably may also be evident in energy spectra. The intensity of this effect will also depend on the slab thickness but additionally on the number of discrete energies as well as the extent of range straggling. This particular ray effect phenomenon and effective mitigation techniques will form the subject of a future report.

Finally, a very attractive feature of our approach is that only moments of the differential cross sections are required. Alternative cross section models that are more accurate than those used for this analysis can easily be employed. The discrete representation of cross sections means that the storage and sampling within the Monte Carlo code remains the same regardless of the angular scattering model or the energy-loss model.

ACKNOWLEDGEMENTS

Sandia is a multiprogram laboratory operated by Sandia Corporation, a Lockheed Martin Company, for the United States Department of Energy under Contract DE-AC04-94AL85000.

REFERENCES

[1] M. J. Berger, "Monte Carlo Calculations of the Penetration and Diffusion of Fast Charged Particles," in *Methods in Computational Physics*, Vol. 1, edited by B. Adler, S. Fernbach and M. Rotenberg, Academic Press, New York (1963).

[2] J. A. Halbleib, R. P. Kensek, T. A. Mehlhorn, G. D. Valdez, S. M. Seltzer and M. J. Berger, "ITS Version 3.0: The Integrated TIGER Series of Coupled Electron/Photon Monte Carlo Transport Codes," Technical Report SAND91-1634, Sandia National Laboratories (1992).

[3] W. R. Nelson, H. Hirayama, and D. W. O. Rogers, "The EGS4 Code System," Technical Report SLAC-265, Stanford Linear Accelerator Center (1985).

[4] J. Baró, J. Sempau, J. M. Fernandez-Varea and F. Salvat, "PENELOPE: An Algorithm for Monte Carlo Simulation of the Penetration and Energy Loss of Electrons and Positrons in Matter," *Nucl. Instrum. Methods Phys. Research*, **B100**, 31 (1995).

[5] J. F. Briesmeister, Editor, "MCNP^{TM} - A General Monte Carlo N-Particle Transport Code, Version 4C," Technical Report LA-13709-M, Los Alamos National Laboratory (2000).

[6] E. W. Larsen, "A Theoretical Derivation of the Condensed History Algorithm," *Ann. Nucl. Energy*, **19**, pp. 701-714 (1992).

[7] I. Kawrakow and A. F. Bielajew, "On the Condensed History Technique for Electron Transport," *Nucl. Instr. Methods* **B 142**, pp. 253-280 (1998).

[8] D. R. Tolar and E. W. Larsen, "A Transport Condensed History Algorithm for Electron Monte Carlo Simulations," *Nucl. Sci. Eng.*, **139**, pp. 47-65 (2001).

[9] C. L. Leakeas and E. W. Larsen, "Generalized Fokker-Planck Approximations of Particle Transport with Highly Forward-Peaked Scattering," *Nucl. Sci. Eng.*, **137**, pp. 236-250 (2001).

[10] A. K. Prinja, V. M. Klein and H. G. Hughes, "Moment Based Effective Transport Equations for Energy Straggling," *Trans. Am. Nucl. Soc.*, **86**, pp. 204-206 (2002).

[11] B. C. Franke, A. K. Prinja, R. P. Kensek and L. J. Lorence, "Discrete Scattering-Angle Model for Electron Pencil Beam Transport," *Trans. Am. Nucl. Soc.*, **86**, pp. 206-208 (2002).

[12] H. W. Lewis, "Multiple Scattering in an Infinite Medium," *Phys. Rev.* **78**, pp. 526-529 (1950).

[13] B. C. Franke, A. K. Prinja, R. P. Kensek and L. J. Lorence, "Ray Effect Mitigation for Electron Transport with Discrete Scattering-Angles," to appear in *Trans. Am. Nucl. Soc.*, **87**, (2002).

[14] C. D. Zerby and F. L. Keller, *Nucl. Sci. Eng.*, **27**, 190 (1967).

[15] G. C. Pomraning, "Higher Order Fokker-Planck Operators," *Nucl. Sci. Eng.*, **124**, 390 (1996).

[16] A. K. Prinja and G. C. Pomraning, "A Generalized Fokker-Planck Model for Transport of Collimated Beams," *Nucl. Sci. Eng.*, **137**, pp. 227-235 (2001).

[17] D. P. Sloan, "A New Multigroup Monte Carlo Scattering Algorithm for Neutral and Charged-Particle Boltzmann and Fokker-Planck Calculations," Technical Report SAND83-7094, Sandia National Laboratories (1983).

[18] J. E. Morel, L. J. Lorence, R. P. Kensek and J. A. Halbleib, "A Hybrid Multigroup/Continuous-Energy Monte Carlo Method for Solving the Boltzmann-Fokker-Planck Equation," *Nucl. Sci. Eng.*, **124**, pp. 369-389 (1996).

[19] R. Evans, *The Atomic Nucleus*, McGraw-Hill, Inc., New York (1976).

[20] L. L. Carter and C. A. Forest, “Transfer Matrix Treatments for Multigroup Monte Carlo Calculations – The Elimination of Ray Effects,” *Nucl. Sci. Eng.*, **59**, pp. 27-45 (1976).

[21] L. Mao, J. P. Both and J. C. Nimal, “Transfer Matrix Treatments in TRIMARAN-II, Nonequally Probable Step Function Representation in Multigroup Monte Carlo,” *Nucl. Sci. Eng.*, **130**, pp. 226-238 (1998).